Measurement 193 (2022) 110945

Contents lists available at ScienceDirect

Measurement

journal homepage: www.elsevier.com/locate/measurement

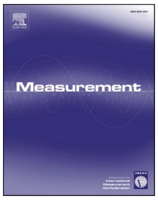

A study of the influence of the sensor sampling frequency on the performance of wearable fall detectors

José Antonio Santoyo-Ramón [a], Eduardo Casilari [b,*], José Manuel Cano-García [c]

[a] Departamento de Tecnología Electrónica, Universidad de Málaga, 29071 Málaga, Spain
[b] Departamento de Tecnología Electrónica, Universidad de Málaga, Instituto TELMA, 29071 Málaga, Spain
[c] Departamento de Tecnología Electrónica, Universidad de Málaga, Instituto TELMA, 29071 Málaga, Spain

ARTICLE INFO

Keywords:
Fall Detection Systems
Human Activity Recognition
Inertial Sensors
Accelerometer
Dataset
Sampling Rate
Convolutional Neural Network
Deep Learning

ABSTRACT

Last decade has witnessed a major research interest on wearable fall detection systems. Sampling rate in these detectors strongly affects the power consumption and required complexity of the employed wearables. This study investigates the effect of the sampling frequency on the efficacy of the detection process. For this purpose, we train a convolutional neural network to directly discriminate falls from conventional activities based on the raw acceleration signals captured by a transportable sensor. Then, we analyze the changes in the performance of this classifier when the sampling rate is progressively reduced. In contrast with previous studies, the detector is tested against a wide set of public repositories of benchmarking traces. The quality metrics achieved for the different frequencies and the analysis of the spectrum of the signals reveal that a sampling rate of 20 Hz can be enough to maximize the effectiveness of a fall detector.

1. Introduction

Falls are a major medical concern, in particular for older adults. The medium and long-term health consequences of falls are directly linked to the time during which the faller remains on the floor unattended [1]. Therefore, it is of great interest, especially for the elderly who live alone, to develop trustworthy alarming systems capable of automatically alerting distant caregivers so that they can provide immediate help whenever a fall is suspected. In this context, during the last decade, the declining hardware costs and the widespread acceptation of wearables have fostered the adoption of these devices in architectures for Fall Detection Systems (FDSs).

The generic purpose of a portable FDS is to discriminate the possible occurrence of a fall accident from any other ordinary movement or ADL (Activities of Daily Living) based on the measurements continuously collected by sensors that can be easily attached to the body or integrated into a garment. Most current wearables (smartwatches, smartbands, etc.) natively embed an IMU (Inertial Measurement Unit) which eases the programming and seamless adoption of fall detection applications into the everyday life of senior citizens.

There is a vast and exhaustive literature focused on the proposal and validation of algorithms designed to identify falls from the inertial signals (especially accelerometry) generated by human movements. The common goal of these proposals is to maximize the efficacy of the classifier to distinguish falls from ADLs. On the contrary, there are far fewer studies that examine the operational aspects of these systems. One of the key elements that may determine the practical feasibility of wearable FDSs is the sampling rate, i.e. the frequency at which the measurements are captured by the inertial sensors to be analyzed by the corresponding fall detection algorithm.

Sampling rate may heavily affect the consumption of the sensors, especially if a gyroscope and a magnetometer are employed [2]. In a practical scenario, the autonomy of a wearable FDS should guarantee a minimum continuous operation of 16–24 h. In other case, the transportable tracking system would have to stop before bedtime to replace or to recharge the battery. Consequently, an unnecessary increase of the energy drain can directly impact on the actual capability of the wearables to act as fall detectors, as they are normally powered with lightweight low-capacity batteries.

Furthermore, the sampling frequency governs the volume of the data stored and processed to generate the detection decision. In this regard, a single accelerometer operating at 200 Hz produces about 2.3 GB of data per day [3]. This aspect is also of great significance if we consider that wearables implementing FDS may also have severe limitations in terms

[*] Corresponding author.
E-mail addresses: jasantoyo@uma.es (J. Antonio Santoyo-Ramón), ecasilari@uma.es (E. Casilari), jcgarcia@uma.es (J. Manuel Cano-García).

https://doi.org/10.1016/j.measurement.2022.110945
Received 31 October 2021; Received in revised form 15 February 2022; Accepted 25 February 2022
Available online 1 March 2022

of memory or computing capacity. The same consideration can be made if the measurements have to be retransmitted (e.g. via Bluetooth) to an external element (e.g. a smartphone) where the detection algorithm is implemented, as frequent wireless transmissions may promptly deplete the battery.

FDSs can be regarded as a particular application of HAR (Human Activity Recognition) systems. In this regard, Gao at al. showed in [4] that increasing the sampling rate above 20 Hz (and up to 50 Hz) improves the recognition accuracy of HAR architectures by just 1% whereas the discrimination capacity of the systems gets stabilized beyond 50 Hz. In fact, many works assume that a sampling rate of 50 Hz is more than sufficient to characterize the human mobility for the identification of physical activities [5].

Contrariwise, in the specific field of FDSs there is not any default rule or consensus to set the sampling frequency. The review presented by Bet et al. in [6] reported that in 75% of the studies on FDSs this frequency is fixed in the interval [40–100] Hz, being 50 Hz the most common value. Even so, there are works where a much higher value is selected (e.g. 800 Hz in [7] or [8]).

The interesting study by Liu et al. in [9] has already analyzed the impact of the sampling rate on the effectiveness of a fall detector system. The work investigated the degradation of the performance of four basic machine learning models (Support Vector Machine -SVM-, k-Nearest Neighbor -kNN-, Naïve Bayes -NB- and Decision Trees -DT-) when the sampling rate of the sensor is modified from 3 to 200 Hz. Results seem to evince that with a rate of 22 Hz most machine learning classifiers can achieve a high accuracy (higher than 97%) to support fall detection systems. In a similar study by Ajerla et al. [3], a Long Short-Term memory (LSTM) network model is employed for fall identification. The system is evaluated with traces captured on the waist and five sampling rates (12.5 Hz, 25 Hz, 50 Hz, 100 Hz, and 200 Hz). From the results and contrary to the previous study, authors conclude that the system is unable to identify falls for frequencies below 50 Hz while no significant improvement is achieved with 100 or 200 Hz.

Silva et al. assessed in [13] the performance of seven fall detection algorithms when a cross-dataset validation is applied, i.e. when the models are tested with a dataset obtained with a scenario, users or body placements of the wearable different from those used to train the classifier. From the study, they deduce that the best performance is achieved by a Random Forest (RF) classifier. The models were fed with a wide set of hand-engineered statistical features computed from the sequence of the acceleration magnitude (corresponding to the measurements gathered during a window of 7.5 s centered in the signal magnitude maximum). In an additional section, authors present a preliminary study of the impact of modifying the sampling frequency (from the original value of 100 Hz to 50, 20, 10, 3 or 1 Hz) on the effectiveness of this optimal RF-based detector. It is observed that a significant decay of performance is only verified for frequencies lower than 10 Hz.

The same approach of Liu and Silva is followed by Zurbuchen et al. in a very recent publication [10]. These authors also investigate the influence of the sampling rate on the detection by observing the behavior of five machine learning classifiers when this parameter is varied. The results of the article seem to indicate that sampling rates over 20 Hz improve system's performance so that a sampling rate of 50 Hz is recommended.

The major drawback of these works is that they employ machine learning classifiers that must be fed with statistical features derived from the measurements. Consequently, the performance of the classifiers employed in these papers strongly rely on the selection (number and typology) of the input features. In order to bypass the problems derived from this election of the input feature set, we propose to extend the previous research by using a deep learning strategy.

In this regard, Convolutional Neural Networks (CNNs) are one of the most popular deep learning architectures. CNNs are formed by a sequence of processing layers of two-dimensional linear convolutional filters. Each layer is normally complemented by a non-linear activation function and a down-sampling (pooling) stage that generate the inputs of the following layer. During the supervised learning phase, based on the analysis of the training dataset, these layers are capable of self-adjusting the filter coefficients to autonomously recognize underlying organizational rules that can represent the data at different scales or abstraction levels. These rules or final features are inputted to a final classifier (typically, a fully connected neural perceptron), which produces the global classification decision.

Deep learning solutions, including CNNs, have been successfully incorporated in the area of HAR systems to replace other conventional machine learning strategies that require a 'hand-crafted' or heuristic selection of features to feed the classifiers [11]. In fact, FDSs have also benefitted from the application of CNNs (see [12] for a review on this topic).

One of the main assets of employing CNNs is that they can be directly fed by the raw data collected by the wearable sensors (e.g. the measurements captured by the accelerometer or the gyroscope). Thus, once the configuration of the classifier is accomplished, the CNN architecture circumvents the need of calculating in real time and in an unsophisticated device complex statistical input features derived from the measurements, as it is required by most machine learning methods.

Another issue of the aforementioned articles on the effect of the sampling rate is that they just study a limited collection of data. The work by Ajerla uses just two repositories: a database (not released) obtained in the laboratory by the authors (containing only 64 falls) and MobiAct [14]. Similarly, the study by Liu also employs only two datasets: one (unpublished too) specifically created from experiments with eight subjects and SisFall repository [15]. The analysis by Silva is in turn based on a single dataset of falls and ADL (AICOS), which is not publicly available (to the best of our knowledge). As it refers to the work by Zurbuchen et al. it only considers SisFall dataset. The use of a wide set of benchmarking databases for the assessment of FDSs is an essential aspect if we take into consideration the noteworthy diversity of the existing repositories. The variety of the included ADLs and falls, the strategies to emulate the falls, the duration of the samples, the characteristics of the participants in the testbed, etc. may clearly influence the performance of the detection algorithm. Thus, a classifier that apparently achieves a good discrimination ratio with a certain dataset may exhibit a much worse behavior with other databases as it has already been shown in [16,17].

In this paper, we employ CNNs to assess the capability of these deep learning architectures to operate as the detection mechanism in a wearable FDS scheme. To this end, we employ 15 public repositories containing mobility traces with the inertial signals caused by ADLs and falls. The time series of the measurements of these datasets are then decimated to reduce the equivalent sampling rate and investigate the impact of this parameter on the effectiveness of the detection decision of the CNN.

The paper is structured as follows: the goals and review of the related literature have been presented in this section. Section 2 describes the utilized procedure for the study of the effects of the sampling rate (selection of the evaluation datasets, configuration and operation of the CNN, utilized performance metrics) whereas Section 3 shows and discusses the obtained results. Finally, the main conclusions are recapitulated in Section 4.

2. Materials and methods

2.1. Election of the datasets

Owing to the inherent complexity of validating FDSs with actual falls, the investigation on fall detection algorithms is normally grounded on samples obtained in a laboratory testbed. Under this validation technique, a group of volunteers must be recruited to execute a set of pre-defined movements (including emulated falls) while transporting one or several inertial sensors on different locations of the body. During the experiments, the signals gathered by the sensors (in the form of time series) are stored in a dataset of traces (manually labelled as ADLs or falls), which are exploited to evaluate the movement classifiers in an offline manner. At present, about 25 of these datasets have been publicly released and are available for the research community as benchmarking tools (see [16] for a comprehensive revision of these datasets).

We discarded for our analysis those databases containing less than 200 movement traces or less than 50 samples of falls (LDPA [18], CGU-BES [19], EVAal [20], UR [21], Gravity project [22], Smartfall [23], SMotion [24]and FARSEEING [25] datasets). We also excluded UniMiB SHAR [26], DLR [27] and Smartwatch [23] databases (because the duration of most samples is too short for the employed observation window employed by the CNN detector) as well as Graz dataset [28] (as it was generated with an accelerometer range of 2 g, which is too low to capture the acceleration peaks caused by falls). After this screening, we finally selected for our study 15 datasets (a number well above that used in the vast majority of works on FDSs). The source and basic properties of these datasets are described in Table 1 while Table 2 indicates the model of the commercial sensing node and the corresponding embedded accelerometer employed to gather the measurements in each dataset, as well as the original sampling rate with which the data were collected. In the table, the term ‘customized design’ refers to the cases where a specific sensing mote was designed and mounted by the authors to produce the dataset. As it can be observed from Table 2, the sampling frequency, which ranges from 18 to 238 Hz, notably diverges depending on the considered dataset. As above mentioned, there is not any commonly accepted rule in the literature to set this parameter and configure the sensors in the testbeds.

2.2. Selection of inputs for the deep classifier

Most algorithms for wearable FDSs base their classification uniquely on the triaxial acceleration signals. In this work we follow this approach for two reasons: firstly, the benefit of combining the information of the accelerometer and another inertial sensors to boost the effectiveness of the fall detectors is an issue still under discussion [42]. Secondly, just some of the datasets selected for the evaluation and described in the previous section include the gyroscope measurements.

Falls result in brusque and abrupt peaks of the acceleration as the subject’s body impacts against the floor [43]. Consequently, to categorize each movement (ADL or fall), the classifier must concentrate its examination of the captured inertial signals on the time interval around the instant where these peaks occurs and a fall can be suspected. For this purpose, we focus the analysis of each trace (ADL or fall) around the point where the maximum of the Signal Magnitude Vector (SMV_i) of the acceleration is found. For the i-th measurement of a certain trace, this magnitude is computable as:

$$SMV_i = \sqrt{A_{x_i}^2 + A_{y_i}^2 + A_{z_i}^2} \tag{1}$$

Being A_{xi} , A_{yi} and A_{zi} the x, y, and z triaxial components captured by the accelerometer. From this sequence, the maximum of the SMV is calculated as:

$$SMV_{max} = SMV_{i_o} = max(\{SMV_i : i \in [1, N]\}) \tag{2}$$

where N is the cardinality of the series, while i_o indicates the index of the sample at which the maximum occurs.

A fall consists of several phases (pre-impact phase, free-fall period, impact, post-fall, etc.), which typically total between 1 s and 3 s [44]. Accordingly, for every trace, we set an observation time interval of 3 s around the maximum (1.5 s before and after the magnitude peak) to incorporate the most significant elements of the dynamics of the movements suspected of being provoked by falls. All the measurements not included in this window are not considered by the classifier to catalogue the trace as fall or ADL.

Therefore, the analysis pattern (A) inputted to the CNN will consist of the time series of the three triaxial components in this time interval:

$$A = \left\{ A_{x_j}, A_{y_j}, A_{z_j} : j \in \left[\left\lceil i_o - \frac{T}{2} f_s \right\rceil, \left\lceil i_o + \frac{T}{2} f_s \right\rceil \right] \right\} \tag{3}$$

where T and f_s respectively designate the duration (3 s) of the observation window around the maximum and the original frequency at which the acceleration was sampled in the corresponding dataset, while the operator $\lceil x \rceil$ round the value of x to the lowest integer greater than x.

With these time series extracted from each series in the dataset we train and test the CNN to assess the classification performance for the

Table 1
Characteristics of the employed datasets.

Dataset & reference	Number of Subjects (Females/ Males)	Number of types of ADLs/ Falls	Number of samples (ADLs/ Falls)	Duration of the samples (s)	Number and positions of the sensing points
AnkFall [29]	21 (5/**16**)	7/4	614 (397/217)	[3.32–19.7]	1: Ankle
Cogent Labs [30]	42 (6/36)	8/6	3302(1476/1826)	[8.36–37.76]	2: Chest, Thigh
CMDFALL [31]	50 (20/30)	15/1	1000 (600/400)	450[1]	2: Waist (left hip), Left wrist
DOFDA [32]	8 (2/6)	5/13	432 (120/312)	1.96–17.262	1: Waist
DU-MD [33]	10 (4/6)	8/2	3299 (2309/990)	[2.85–11.55]	1: Wrist
Erciyes Univ. [34]	17 (7/10)	16/20	3302(1476/1826)	[8.36–37.76]	6: Chest, Head, Ankle, Thigh, Wrist, Waist
FallAllD [35]	15 (7/8)	44/35	6605 (4883/1722)	20	3: Waist, Wrist, Chest (lanyard around the neck)
IMUFD [36]	10 (n.i.[2])	8/7	600(390/210)	[15–20.01]	7: Chest, Head, Left ankle, Left thigh, Right ankle, Right thigh, Waist
KFall [37]	32 (0/32)	21/15	5075(2729/2346)	[2.03–40.86]	1: Waist (low back)
MobiAct [14]	57(15/42)	9/4	2526 (1879/647)	[4.89–300.01]	1: Thigh (pocket)
SisFall [15]	38 (19/19)	19/15	4505 (2707/1798)	[9.99–179.99]	1: Waist
tFall [38]	10 (3/7)	d.r.[3]/8	10,909 (9883/1026)	6 (all samples)	1: Hand bag
TST [39]	11 (n.i.)	4/4	264 (132/132)	[3.84–18.34]	2: Waist, Wrist
UMAFall [40]	19 (8/11)	12/3	746 (538/208)	15 (all samples)	5: Ankle, Chest, Thigh, Waist, Wrist
UP-Fall [41]	17 (8/9)	6/5	559(304/255)	[9.409–59.979]	5: Ankle, Neck, Thigh (pocket), Waist, Wrist

[1] For CMDFAL dataset, all the 20 programmed movements are executed in a continuous manner during 7.5 min.

[2] n.i.: not indicated in the article.

[3] d.r.: ADLs were captured during the actual daily life of the volunteers and then split into different not specified actions.

Table 2
Models of the sensing mote and accelerometer employed in each dataset.

Dataset	Mote model	Accelerometer model	Sampling rate (Hz)
AnkFall	Customized design	Analog devices ADXL345	50
Cogent Labs	SHIMMER	NXP MMA7260Q	100
CMDFALL	WAX3 mote	WAX3	50
DOFDA	Customized design	Analog devices ADXL345	33
DU-MD	Trillion Node Engine mote	STMicroelectronics LIS2DH	33
Erciyes Univ.	XSens MTw mote	Not indicated by the vendor	25
FallAllD	RF-TRACK data logger (	STMicroelectronics LSM9DS1	238
IMUFD	ADPM Opal mote	Not indicated by the vendor	128
KFall	Customized design	STMicroelectronics LPMS-B2	100
MobiAct	Samsung Galaxy S3 phone (acc.)	STMicroelectronics LSM330DLC	87
SisFall	Customized design	Analog devices ADXL345	200
tFall	Samsung Galaxy Mini (smartphone)	InvenSense MPU6500	45
TST	SHIMMER mote	NXP MMA7260Q	100
UMAFall	Thigh: Samsung S5 (smartphone) Rest: Texas Instruments Sensortag	InvenSense MPU6500 InvenSense MPU-9250	100 (Thigh) 20 (Rest)
UP-Fall	Mbientlab MetaSensor Mote	Bosch BMI160 3-axis IMU	18

reference or ‘baseline’ case, i.e. the case in which the traces are not subsampled and the original sampling rate is used to represent the movements.

Once this baseline performance is obtained, we decimate the measurements in the datasets to analyze the impact of reducing the sampling frequency. In this scenario, for a certain trace, the new network input ($A^{[k]}$) will be formed by the subsampled series of the triaxial components:

$$A^{[k]} = \{A^{[k]}_{x_l}, A^{[k]}_{y_l}, A^{[k]}_{z_l}\} \tag{4}$$

where k indicates the factor with which the series are decimated. For the x-axis the subsampled series of the acceleration component can be computed as:

$$A^{[k]}_{x_l} = \left\{ A_{x_{\left(\left\lceil i_O - \frac{T}{2} f_S \right\rceil + (l-1) \bullet k\right)}} : l \in \left[1, \left\lceil \frac{T \bullet f_s + 1}{k} \right\rceil\right] \right\} \tag{5}$$

while the decimated series for the other axes ($A^{[k]}_{y_l}$ and $A^{[k]}_{z_l}$) are calculated in an identical manner.

For each dataset, the analysis is repeated for different values of the decimation factor (k), ranging from 2 to the maximum integer value (k_{max}) that guarantees that a minimum effective sampling rate $\left(\frac{f_s}{k}\right)$ of 1 Hz is achieved:

$$k \in \{2, 3, \cdots k_{max}\} \forall k \in \mathbb{N} : \frac{\mathrm{f_s}}{\mathrm{k}} \geq 1 \quad \mathrm{Hz} \tag{6}$$

2.3. Configuration of the CNN

The CNN was implemented by means of scripts through the Matlab framework provided by the Deep Learning ToolboxTM [45]. As this toolbox is mainly oriented to process images, in order to input the triaxial acceleration data, we utilized an equivalent ‘image’ with three equivalent´channelś (one channel per each axis of the accelerometer measurements) and a dimension of (1 × *width*) ‘pixels’, where *width* indicates the number of samples of each axis contained in the observation window (which, in turn, depends on both the sampling frequency of each dataset and the decimation factor). The values of the acceleration measurement are z-score normalized before feeding the classifier.

The optimal configuration of the hyperparameters of the CNN was achieved by massive grid search. To that end, more than 4500 combinations of candidate values for the tuning parameters were tested aimed at maximizing the average performance of the network for all the considered datasets. The final structure and dimension of the deep learning classifier is sketched in Fig. 1. The rest of the hyperparameters are tabulated in Table 3. As it is shown in the figure, automatic feature extraction is accomplished through five ‘hidden’ layers (o convolutional blocks) including a convolutional layer, a batch normalizer, a ReLu Activation and a Max Pooling layer. In the final stage, the extracted features feed a fully connected neural layer with a Softmax activation function. This operation assigns to every input a probability distribution of the mutually exclusive class (ADL or fall), which is used by a cross-entropy cost function to generate the classification decision.

To validate the generated models, a classical 5-fold cross-validation technique was carried out. Thus, each repository was split into five partitions with the same quantity of traces. This division of the traces was performed at random but guaranteeing that every partition includes a similar number of samples from the different movement types and from all the experimental users. The training and test of the CNN is iterated five times. For each iteration, a different partition is reserved for testing while the other four are used for training (three partitions) and validation (one partition). The mean values of the performance metrics (described in the next Sections 2.4) obtained for the five repetitions are then calculated to characterize the effectiveness of the classifier.

2.4. Performance metrics

From the decisions taken by the CNN during the test phase, we compute two metrics commonly used to evaluate the behavior of binary classifiers: the sensitivity (*Se*), which characterizes the capability of the FDS to identify falls, and the specificity (*Sp*), which describes the efficacy of the detector to avoid false alarms (ADLs misidentified as falls).

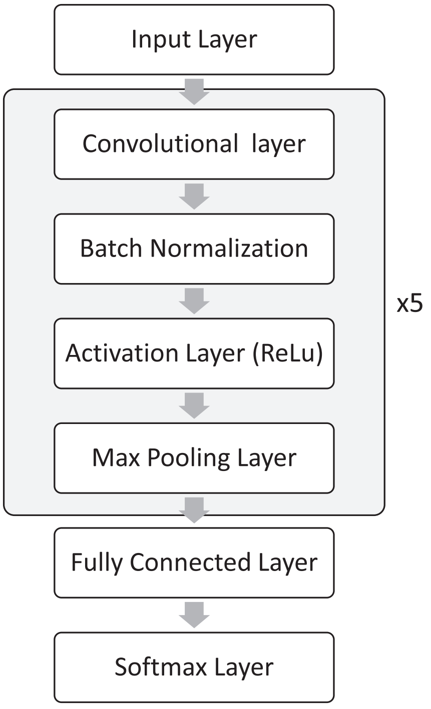

Fig. 1. Structure of the employed CNN.

Table 3
Hyperparameters and configuration of the CNN.

Network Dimensioning and Structure	
Number of feature extraction layers	5
Sub-layers for every extraction layer	4 (1 normalization, 1 convolutional, 1 activation and 1 max pooling layer)
Number of filters for each convolutional layer	64
Filter size for the convolutional layers	1x8
Size of zero-padding	4 samples
Stride	1x1 ("non-strided")
Final classification layer	Fully connected layer with a final activation function and a classifier
Layer activation functions	ReLU (feature extraction layers) and softmax (output layer)
Method and configuration of the training procedure	
Training algorithm	Stochastic Gradient Descent Momentum
Mini-batch size[1]	64 training instances
Maximum number of training epochs[2]	100
Validation patience	5 epochs
Tecniques to prevent overfitting	Validation, L2 Regularization
Initial learning rate	0.01

[1] These batches are used to estimate the gradient of the loss in every iteration.
[2] Training stops before this value is achieved if overfitting is detected through the validation set.

These metrics are typically computable as the following ratios:

$$Se = \frac{TP}{TP + FN} \tag{7}$$

$$Sp = \frac{TN}{TN + FP} \tag{8}$$

where *TP, TN, FP* and *FN* respectively define the number of true positives (well identified falls), true negatives (well classified ADLs), false positive (or false alarms) and false negatives (unidentified falls) obtained after applying the detector to the test subsets. In contrast with other typical metrics (such as accuracy), *Se* and *Sp* are not inherently affected by the unbalance nature of the datasets (i.e. the different number of traces of ADLs and falls).

Since sensitivity and specificity are negatively correlated, we also employ the mean geometric of these two parameters ($\sqrt{Se \cdot Sp}$) as a single descriptor of the global system performance.

3. Results and discussion

3.1. Results for the original sampling frequencies

As a baseline reference for the study of the subsequent sections, we obtained the performance metrics achieved when the CNN is trained and tested with the original sequences of the datasets (without any subsampling).

In the case of datasets containing the measurements captured on different body locations, the behavior of CNN is individually assessed for each position, that is to say, the analysis is repeated for each measurement point with independence of the time series collected on other body locations for the same movements.

The results (sensitivity, specificity and geometric mean of both parameters) of the application of the classifier for all the repositories and sensing locations are summarized in Table 4. To offer an insight of the statistical confidence of the performance achieved by the CNN, in the last two columns, the table incorporates the mean and standard deviation of the global performance metric ($\sqrt{Se \cdot Sp}$), computed from the 5-fold cross-validation, as well as the corresponding 95% confidence interval.

Except for DU-MD repository (which contains a group of ADL traces with an anomalous behavior) and, to a lesser extent, tFall dataset, the global computed quality metric achieves values higher than 0.9. Moreover, in 10 out of the 15 employed repositories, the global metric (geometric mean of specificity and sensitivity) is above 0.95, while for all datasets (except DU-MD) the obtained maximum specificity exceeds 95%, which evinces the efficacy of the classifier to avoid false alarms.

Thus, the measured effectiveness of CNN as a binary classifier for fall detection is in general superior or at least comparable with other detectors based on machine learning techniques that have been proposed by the related literature (see, for example, the state-of-the-art presented in the review articles [12,46–50]).

As it refers to the analysis of the best position to locate a fall detector, the analysis of the results reached for the datasets containing multiple simultaneous sensing point (especially Erciyes, IMUFD, UMAFall and UP-Fall databases) shows that the efficacy of the classifier is maximized when the CNN is inputted with the signals captured on the waist or chest. This finding is coherent with the literature on FDS and posture recognition in general. Indeed most studies on this topic such as [51–54] suggest that the optimal position of a inertial sensor for a FDS or HAR system is waist (chest is normally considered to be a more inadequate location to transport a wearable sensor due to ergonomics). Chest and waist are closer to body's Center of Gravity (COG),so the inertial measurements captured on those points describe the global mobility of the user better than those collected by sensors on the limbs (wrist, ankle), which may exhibit local motion patterns far more independent of the general activity or position of the body.

3.2. Results for the decimated sequences

We now focus our attention on the impact of the sampling frequency on the previous results. In particular, we repeat the experiments (training and testing the CNN) with all the datasets when this parameter is modified. For this purpose, as commented in section 2.2, we diminish the effective sampling rate by decimating the series of the accelerometer measurements by a certain integer factor (k). Again, when a dataset includes the traces captured at different body positions, the classifier is applied and tested individually with the samples collected on each possible sensor location.

The results achieved by the neural classifier as a function of the employed equivalent sampling frequencies are represented in the graphs of Figs. 2 and 3. In particular, each graph simultaneously shows the global metric ($\sqrt{Se \cdot Sp}$) obtained with the series captured on a certain sensor location for all the datasets that utilized that position to place the inertial measurement unit. Thus, Fig. 2 includes the performance computed for the series measured on the ankle (graphs a & b), chest (graphs c & d), head (graphs e & f) and thigh or trouser packet (graphs g & h), while Fig. 3 depicts the same metric for the traces on the waist (graphs a & b), wrist (graphs c & d) and handbag (graphs e & f). In both figures, the graphs on the left illustrate the performance of the CNN for all the considered sampling rates (original and decimated values) in each repository. As the number of tested sampling rates differ from one dataset to another, aiming at providing a better understanding and comparison of the curves, the graphs on the right detail the behavior of the detector for sampling rates between 1 and 15 or 20 Hz. To avoid hampering the readability and understandability of the curves, the figures do not include the error bars or any other information describing the uncertainty of the quality metric. However, the range of the obtained confidence intervals were very similar to those reached for the baseline case (see Table 4).

From the figures, we clearly observe that for all datasets and all the considered sensor placements the efficacy of the classifier only begins to decrease for sampling rates lower than 10–15 Hz. Except for the case of the traces in DU MD datasets and for the series of CMDUFALL captured

Table 4
Results for the baseline case (without subsampling).

Dataset	Position	*Se*	*Sp*	$\sqrt{Se\bullet Sp}$	95% Confidence Interval
AnkFall	Ankle	0.9290	0.9971	0.9623 ± 0.0155	[0.9431, 0.9815]
CMDFALL	Hip	0.8841	0.9667	0.9237 ± 0.0225	[0.8958, 0.9516]
	Wrist	0.7568	0.9100	0.8289 ± 0.0448	[0.7733, 0.8845]
Cogent Labs	Chest	0.9884	0.9943	0.9913 ± 0.0095	[0.9795, 1.0000]
	Thigh	0.9616	0.9957	0.9784 ± 0.0150	[0.9598, 0.9970]
DOFDA	Waist	1.0000	0.9750	0.9871 ± 0.0289	[0.9512, 1.0000]
DU MD	Wrist	0.5843	0.9217	0.6582 ± 0.3873	[0.1772, 1.0000]
Erciyes	Chest	0.9940	0.9939	0.9939 ± 0.0032	[0.9899, 0.9979]
	Head	0.9912	0.9918	0.9915 ± 0.0037	[0.9869, 0.9961]
	Right ankle	0.9884	0.9918	0.9901 ± 0.0024	[0.9871, 0.9931]
	Right thigh	0.9951	0.9986	0.9968 ± 0.0020	[0.9944, 0.9993]
	Right wrist	0.9890	0.9905	0.9897 ± 0.0036	[0.9853, 0.9942]
	Waist	0.9984	0.9973	0.9978 ± 0.0018	[0.9956, 1.0000]
FallAllD	Waist	0.8597	0.9679	0.9122 ± 0.0147	[0.8940, 0.9304]
IMUFD	Chest	0.9616	0.9763	0.9689 ± 0.0151	[0.9502, 0.9876]
	Head	0.9761	0.9838	0.9798 ± 0.0105	[0.9668, 0.9928]
	Left ankle	0.9233	0.9575	0.9402 ± 0.0179	[0.9179, 0.9624]
	Left thigh	0.9142	0.9786	0.9455 ± 0.0286	[0.9100, 0.9810]
	Right ankle	0.9384	0.9493	0.9435 ± 0.0181	[0.9210, 0.9660]
	Right thigh	0.9519	0.9865	0.9689 ± 0.0061	[0.9614, 0.9765]
	Waist	0.9335	0.9736	0.9532 ± 0.0276	[0.9189, 0.9874]
KFall	Waist	0.9983	0.9996	0.9989 ± 0.0011	[0.9976, 1.0000]
MobiAct	Trouser pocket	0.9234	0.9946	0.9578 ± 0.0379	[0.9107, 1.0000]
SisFall	Waist	0.9883	0.9966	0.9925 ± 0.0052	[0.9860, 0.9989]
tFall	Hand bag: Left side	0.8032	0.9892	0.8903 ± 0.0446	[0.8349, 0.9457]
TST	Right wrist	0.9529	0.9667	0.9593 ± 0.0398	[0.9099, 1.0000]
	Waist	0.9843	0.9742	0.9791 ± 0.0145	[0.9611, 0.9972]
UMAFall	Ankle	0.9322	0.9505	0.9408 ± 0.0112	[0.9269, 0.9548]
	Chest	0.9733	0.9841	0.9786 ± 0.0111	[0.9648, 0.9924]
	Right Trouser pocket	0.9255	0.9841	0.9542 ± 0.0122	[0.9390, 0.9694]
	Waist	0.9730	0.9895	0.9811 ± 0.0211	[0.9549, 1.0000]
	Wrist	0.8763	0.9761	0.9246 ± 0.0241	[0.8947, 0.9546]
UP-Fall	Ankle	0.9822	0.9912	0.9867 ± 0.0122	[0.9715, 1.0000]
	Neck	0.9661	0.9957	0.9806 ± 0.0103	[0.9678, 0.9934]
	Right thigh (pocket)	0.9703	0.9752	0.9725 ± 0.0280	[0.9378, 1.0000]
	Waist (belt)	0.9849	0.9829	0.9837 ± 0.0173	[0.9623, 1.0000]
	Wrist	0.9245	0.9747	0.9491 ± 0.0208	[0.9232, 0.9749]

on the wrist, in all the tests the global quality metric keeps stable above 0.95 for sampling rates higher than 15 Hz. In some cases (see, for example, the behavior for the measurements collected on the hand bag in Fig. 3.e), results indicate that reducing the sampling rate even increases the capacity of the classifier to discriminate falls from ADLs. This could be explained by the fact that a sampling rate lower than the original one reduces the dimension of the input vectors of the classifier, which in turn may ease the self-configuration and capability of generalization of the deep learning model for convolutional filters of a fixed dimension.

3.3. Results with a low-pass filter

To confirm the relevance of the low frequency components in the characterization of the activities, we repeat the baseline experiment (with no subsampling) by feeding the CNN with the time series of the triaxial acceleration when they are previously low-pass filtered to remove the high frequency content in the signals. For this task, we employ a basic minimum-order filter with a stopband attenuation of 60 dB and three possible passband frequencies (f_c): 5, 10 and 20 Hz. When implementing the filter, the selected cut-off frequency must be lower than the half of the sampling frequency (f_s) so that the Nyquist theorem is always fulfilled. Accordingly, the passband frequencies of 10 Hz and 20 Hz cannot be applied to those datasets with an original sampling rate of 18 Hz (UP-Fall repository) or 20 Hz (four sensor positions in UMAFall dataset).

The results (geometric mean of sensitivity and specificity) of this testbed with the filtered signals for the three values of f_c, all the datasets and all the sensor placements are presented in Table 5. The table also includes the performance attained by the baseline case when no filter is applied to the collected traces. From the table, we observe than just in very few cases and for the lowest passband frequency (5 Hz), a certain degradation of the quality metric is caused by the filtering process. In the table, those cases (with a decrease of the global metric higher than 3% with respect to the reference experiment) are marked in italics. Conversely, for most repositories and positions, the CNN behaves better (results highlighted in bold) than in the baseline case when the signals are low pass filtered with a cut off frequency of 10 or 20 Hz (an even 5 Hz). From this analysis, we can again conclude that a sampling rate of 20 Hz, which permits a proper characterization of frequency components below 10 Hz, is enough to provide the classifier with the minimum information to differentiate falls and ADLs.

3.4. Study of the power spectrum of the signals

Previous results visibly indicate that the significant frequency components required to classify ADLs and falls concentrate on a frequency band between 0 and 10 Hz. To corroborate this fact, we examine the distribution of the power spectrum of the acceleration magnitude. In Table 6, we display the average percentage of the total signal power in two low frequency ranges: [0–2.5 Hz] and [0–5 Hz] for all datasets and for all the body locations of the sensors. In the table, we separately analyze the power concentration for ADLs and Falls. For comparison purposes, we extend the analysis to the movement traces existing in DaLiAc dataset [55], which includes 13 types of real-life ADLs, as well as those in the already mentioned FARSEEING [25] repository. This database is exclusively composed of 22 actual falls captured during a long-term monitoring of a group of community-dwelling older adults and

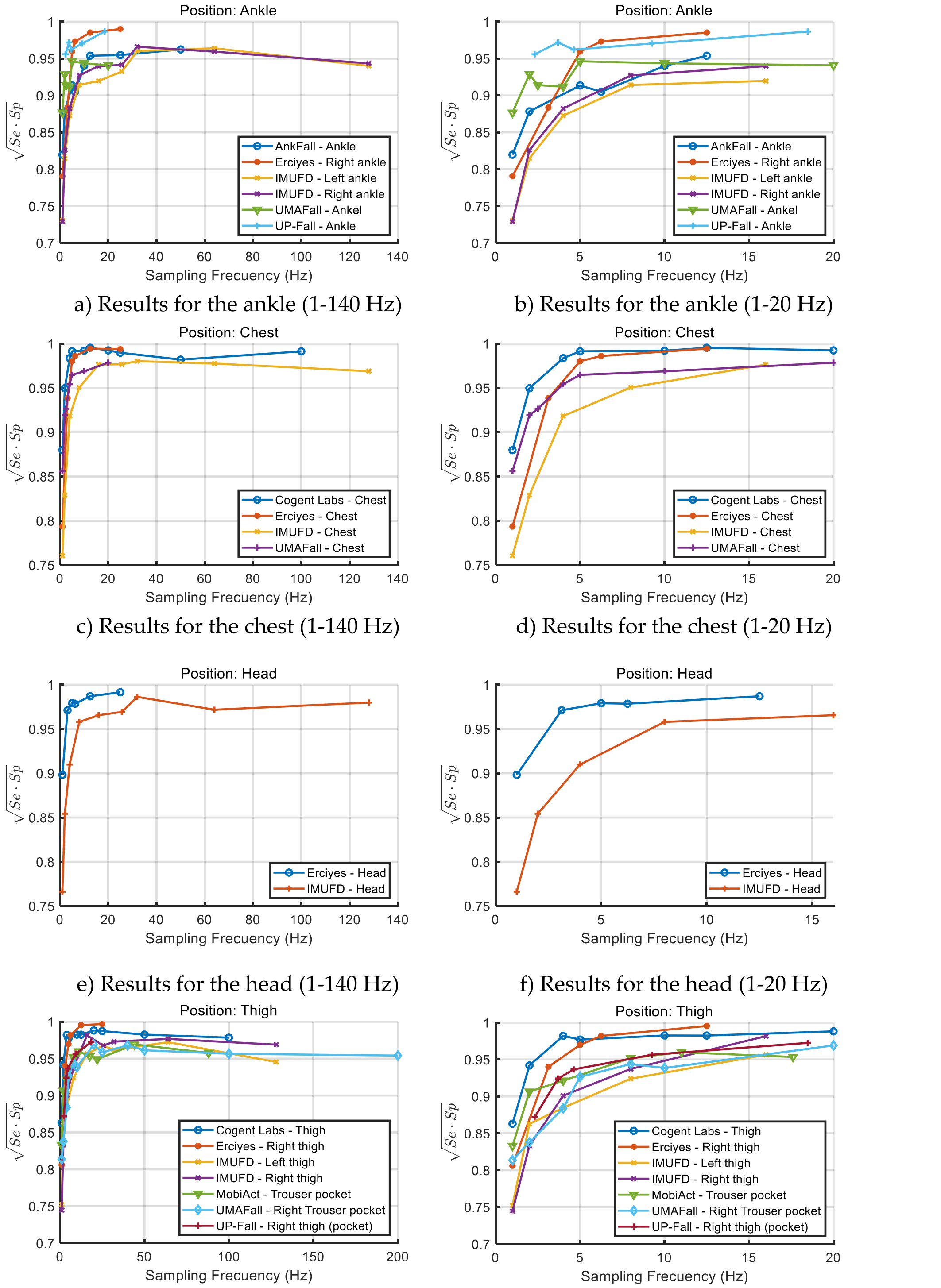

a) Results for the ankle (1-140 Hz)

b) Results for the ankle (1-20 Hz)

c) Results for the chest (1-140 Hz)

d) Results for the chest (1-20 Hz)

e) Results for the head (1-140 Hz)

f) Results for the head (1-20 Hz)

g) Results for the thigh/trouser pocket (1-140 Hz)

h) Results for the thigh/trouser pocket (1-20 Hz)

Fig. 2. Evolution of the global quality metric (geometric mean of the of the sensitivity and specificity) achieved by the deep learning classifier as a function of the employed accelerometer sampling rate and the position of the considered sensor in each dataset: ankle (graphs a & b), chest (graphs c & d), head (graphs e & f), thigh or trouser packet (graphs g & h). Graphs on the left (a, c, e & g) show the performance for all the considered sampling rates in each repository. Graphs on the right (b, d, f & h) detail the behavior of the classifier for sampling rates in the range [0–15 Hz] or [0–20 Hz].

patients with high-risk of falling.

From Table 6, we observe that for the ADLs, the average percentage of power in the [0–5 Hz] band ranges between 91.15 and 99.38% depending on the datasets and body locations. For the [0–2.5 Hz] band these percentages vary from 87.70% to 98.38%.

As it could be expected, high frequency components have a higher weight on the spectral density of the acceleration signals of falls, as these accidents are associated to brusque and sudden changes of the angle and speed on both the limbs and the trunk. However, the relevance of the low frequencies is still noteworthy for falls, as the average fraction of power in the [0–5 Hz] band is between 83.46% and 97.97% for all the experiments.

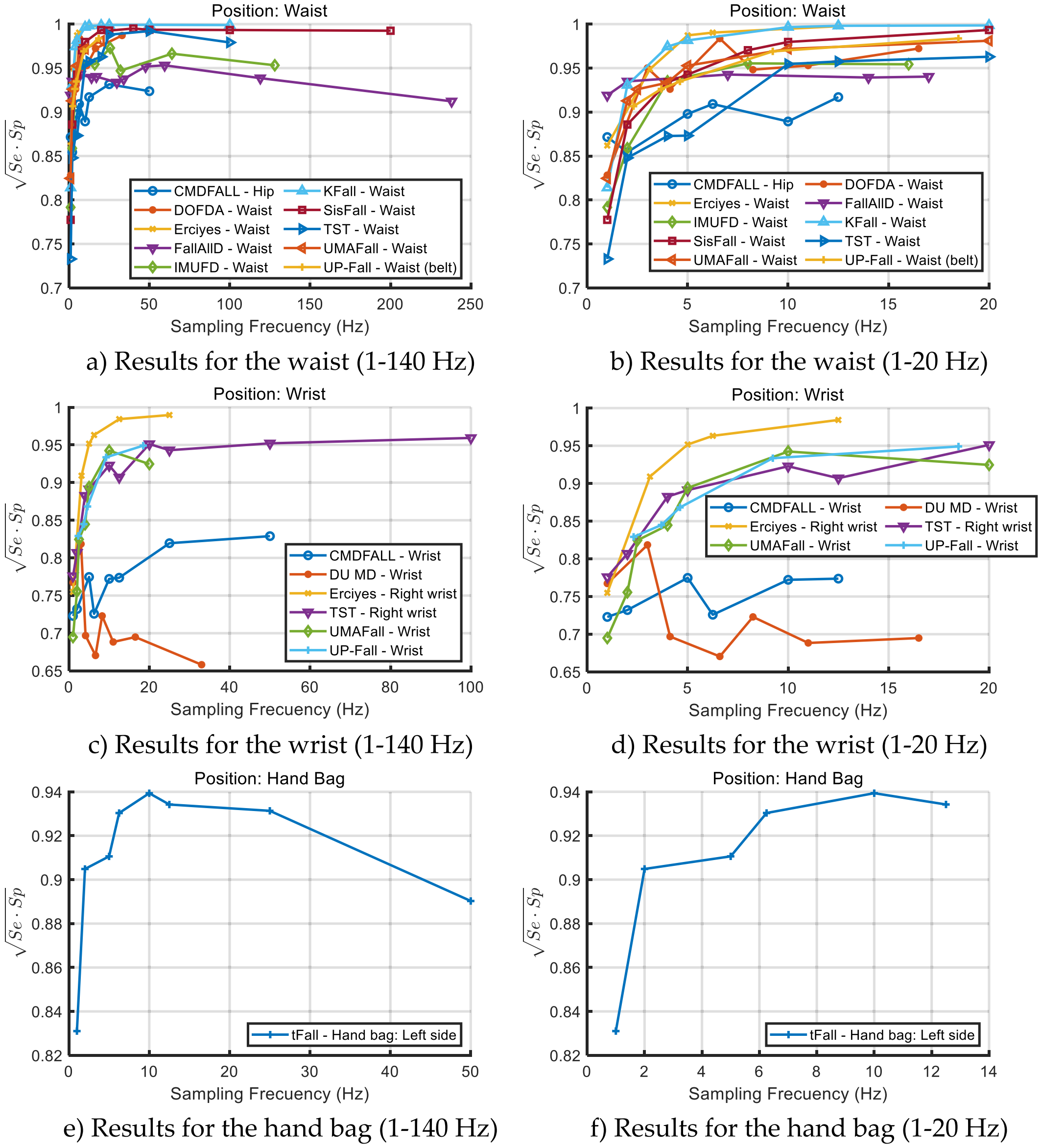

a) Results for the waist (1-140 Hz)

b) Results for the waist (1-20 Hz)

c) Results for the wrist (1-140 Hz)

d) Results for the wrist (1-20 Hz)

e) Results for the hand bag (1-140 Hz)

f) Results for the hand bag (1-20 Hz)

Fig. 3. Evolution of the global quality metric (geometric mean of the of the sensitivity and specificity) achieved by the deep learning classifier as a function of the employed accelerometer sampling rate and the position of the considered sensor in each dataset: waist (graphs a & b), wrist (graphs c & d), hand bag (graphs e & f). Graphs on the left (a, c &e) show the performance for all the considered sampling rates in each repository. Graphs on the right (b, d & f) detail the behavior of the classifier for sampling rates in the range [0–15 Hz] or [0–20 Hz].

Graphs in Fig. 4 verify a rapid decay with frequency of the power spectrum for both ADLs and falls (even though this decay is always slower for falls). For the sake of simplicity, the figure only depicts the results corresponding to the series captured on the waist (hip in the case of DaLiAC repositories) although similar results are achieved if the study focuses the signals captured on other body positions.

These results are consistent with other previous studies that have analyzed the biomechanics of ADLs. Mathie et al. showed in [56] that the main energy band for daily activities is in the frequency interval from 0.3 and 3.5 Hz. According to Antonsson and Mann [57], 99% of the power of the acceleration signal in gait is contained in the band below 15 Hz. Similarly, in [58] Winter reported that walking concentrates 99.7% of the signal power below 6 Hz. This author proposes using a 1st order Butterworth low-pass filter with a cutoff frequency of 20 Hz to remove noise caused by diverse sources (the sensor, the precision of the digitizer or human errors). Nguyen et al. have also demonstrated in [59] that during a TUG (Timed-Up-and-Go) routine, which comprises four common ADLs (standing, walking, turning and sitting), the dominant frequencies of the inertial signals focus in the band below 10 Hz. In this vein, Bouten et al. conclude in [60] that 20 Hz is enough to for the assessment of ADLs. From our own results, we can conclude that this recommendation can be extended to fall detection systems

4. Conclusions

In spite of the extensive literature on wearable fall detection systems (FDSs), there are some practical aspects for the actual implementations of these human activity classifiers which have been disregarded by most studies. Wearables usually present heavy restrictions in terms of computing power, memory, battery capacity or transmission speed. In this regard, the sampling rate set in the inertial measurement unit embedded in these devices may severely influence the viability of a wearable fall detector in a real application scenario. This article has presented a thorough analysis of the impact of the sampling frequency on the performance of wearable fall detection systems based on acceleration signals. As the decision algorithm, we employed a convolutional

Table 5
Global metric ($\sqrt{Se\cdot Sp}$) obtained when the input acceleration sequences are low-pass filtered (bold figures denote those cases in which the use of the low-pass outperforms the baseline case with no filtering while italics indicate those situations in which the filtered signals decreases the performance metric of the baseline case more than 3%).

Dataset	Sensor position	No filter	$f_c = 5$ Hz	$f_c = 10$ Hz	$f_c = 20$ Hz
AnkFall	Ankle	0.9623	0.9595	**0.9636**	0.9455
CMDFALL	Hip	0.9237	*0.8844*	0.9136	0.9225
	Wrist	0.8289	*0.7636*	**0.8519**	**0.8318**
Cogent Labs	Chest	0.9913	**0.9968**	0.9911	0.9865
	Thigh	0.9784	**0.9828**	**0.9829**	**0.9826**
DOFDA	Waist	0.9871	0.*9131*	**1.0000**	–
DU MD	Wrist	0.6582	**0.7428**	0.4836	–
Erciyes	Chest	0.9939	**0.9959**	**0.9954**	–
	Head	0.9915	**0.9920**	0.9892	–
	Right ankle	0.9901	**0.9936**	**0.9936**	–
	Right thigh	0.9968	**0.9974**	0.9968	–
	Right wrist	0.9897	**0.9918**	**0.9918**	–
	Waist	0.9978	0.9975	0.9966	–
FallAllD	Waist	0.9122	0.9032	**0.9309**	**0.9265**
IMUFD	Chest	0.9689	**0.9711**	**0.9777**	**0.9694**
	Head	0.9798	0.9637	0.9750	**0.9800**
	Left ankle	0.9402	*0.9054*	0.9396	**0.9431**
	Left thigh	0.9455	**0.9678**	0.9349	**0.9501**
	Right ankle	0.9435	*0.9068*	0.9291	0.9344
	Right thigh	0.9689	0.9650	0.9605	0.9648
	Waist	0.9532	**0.9654**	**0.9714**	**0.9614**
KFall	Waist	0.9989	0.9975	0.9986	0.9987
MobiAct	Trouser pocket	0.9578	0.9422	**0.9614**	**0.9616**
SisFall	Waist	0.9925	**0.9951**	**0.9941**	**0.9925**
tFall	Hand bag: Left side	0.8903	**0.9170**	**0.9259**	**0.9096**
TST	Right wrist	0.9593	0.*9188*	0.9462	0.9346
	Waist	0.9791	0.9656	0.9585	0.9596
UMAFall	Ankle	0.9408	**0.9573**	–	–
	Chest	0.9786	0.9757	–	–
	Right Trouser pocket	0.9542	**0.9557**	0.9424	0.9509
	Waist	0.9811	**0.9864**	–	–
	Wrist	0.9246	**0.9634**	–	–
UP-Fall	Ankle	0.9867	0.9619	–	–
	Neck	0.9806	**0.9823**	–	–
	Right thigh (pocket)	0.9725	**0.9766**	–	–
	Waist (belt)	0.9837	0.9687	–	–
	Wrist	0.9491	0.9298	–	–

Table 6
Average percentage of the total signal power in two low frequency ranges (0–2.5 Hz, and 0–5 Hz) for ADLs and falls.

Dataset	Position	ADL (0–2.5 Hz)	ADL (0–5 Hz)	Falls (0–2.5 Hz)	Falls (0–5 Hz)
AnkFall	Ankle	87.70%	91.15%	80.35%	86.59%
CMDFALL	Hip	94.40%	96.74%	84.21%	88.77%
	Wrist	93.87%	97.21%	77.28%	83.78%
Cogent Labs	Chest	97.15%	98.94%	86.49%	93.10%
	Thigh	94.72%	96.29%	89.33%	94.97%
DOFDA	Waist	96.62%	98.66%	74.81%	84.70%
DU MD	Wrist	98.24%	99.53%	85.04%	90.99%
Erciyes	Chest	96.93%	98.05%	91.91%	96.90%
	Head	96.58%	98.21%	88.30%	94.60%
	Right ankle	98.35%	99.24%	84.86%	93.70%
	Right thigh	98.38%	99.38%	85.74%	94.48%
	Right wrist	97.55%	99.02%	80.04%	89.37%
	Waist	98.04%	99.23%	86.89%	96.68%
FallAllD	Waist	92.84%	95.92%	80.84%	86.50%
IMUFD	Chest	95.41%	98.07%	84.93%	91.57%
	Head	94.04%	96.69%	84.42%	92.01%
	Left ankle	87.14%	91.91%	76.94%	84.31%
	Left thigh	88.83%	91.76%	79.07%	86.33%
	Right ankle	87.37%	91.95%	75.90%	83.46%
	Right thigh	89.42%	92.25%	79.03%	86.79%
	Waist	95.85%	97.61%	84.20%	90.62%
KFall	Waist	93.7748%	96.998%	82.6078%	93.5115%
MobiAct	Trouser pocket	95.65%	97.88%	91.22%	95.90%
SisFall	Waist	94.15%	96.87%	76.29%	85.59%
TST	Right wrist	96.62%	98.3%	84.27%	91.91%
	Waist	93.09%	95.73%	74.1%	86.84%
UMAFall	Ankle	92.86%	96.25%	82.74%	91.95%
	Chest	96.63%	98.62%	89.33%	94.97%
	Right Trouser pocket	94.07%	96.19%	86.62%	92.81%
	Waist	’95.36%	97.66%	82.61%	93.28%
	Wrist	91.95%	96.14%	81.82%	91.18%
UP-Fall	Ankle	97.49%	99.35%	90.31%	97.32%
	Neck	96.39$	98.9%	92.96%	97.97%
	Right thigh (pocket)	96.98%	99.1%	90.74%	97.41%
	Waist (belt)	95.73%	98.56%	90.68%	97.20%
	Wrist	96.26%	98.88%	91.11%	97.41%
tFall	Hand bag: Left side	94.93%	97.29%	89.81%	95.19%
DALIAC (ADLs)	Hip	90.54%	92.95%	–	–
FARSEEING (Falls)	Waist	–	–	77.72%	87.36%

neural network (CNN), which is trained and hyper-parametrized to discriminate falls from ordinary movements or ADL (Activities of Daily living). The use of a deep learning strategy avoids the need of selecting and defining a set of input features (as it is required by other machine learning architectures), which may determine the behavior of the detector with respect to the selected sampling rate. Thus, the classifier is directly fed with a sequence of the raw measurements collected by the accelerometer during observation time windows of 3 s around the acceleration peaks.

The CNN is initially evaluated (trained, validated and tested) with the traces provided by 15 different public datasets conceived as a benchmarking tool for the assessment of fall detection algorithms. The study of the performance with the original sampling rates shows the high adaptability of the classifier to accurately discriminate falls and ADLs (with sensitivities and specificities higher than 0.95) for nearly all datasets and almost with independence on the position of the sensors with which the samples were captured. Once this baseline case is analyzed and taken as a reference, we repeated the experiments but now reducing the sampling rate of the series through a simple decimation technique. Thus, the CNN is re-trained and re-evaluated with these new sampling frequencies and for all the databases and sensor locations. Results clearly bring to light that the system performance only degrades when the sampling rate is set to a value in the range of 10–15 Hz. Moreover, the detection ratio improves in many cases when the original rate is reduced to values between 20 and 40 Hz. This phenomenon could be explained by the reduction of the data array with the measurements required at the input of the classifier, since an unnecessary increase in the input features and complexity of a neural model normally leads to overfitting the training patterns.

These results are confirmed when no decimation is applied to the series but instead the triaxial acceleration signals are low pass filtered before being inputted to the CNN. The irrelevance of the frequency components in the band higher than 10 Hz is also proved when the power spectrum of the acceleration module for both ADLs and falls is assessed. Even in the case of falls, the power density rapidly decreases

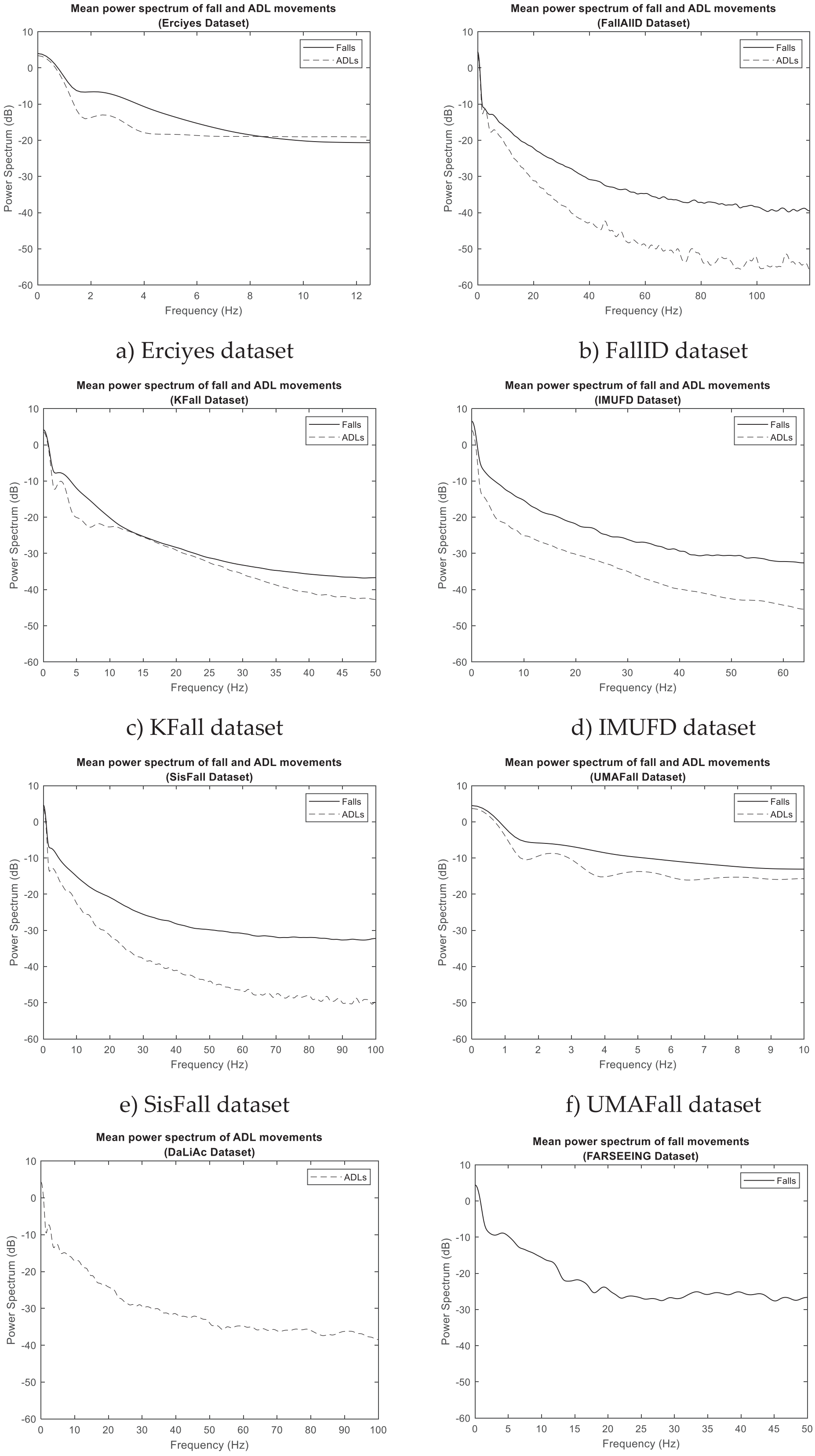

a) Erciyes dataset

b) FallID dataset

c) KFall dataset

d) IMUFD dataset

e) SisFall dataset

f) UMAFall dataset

g) DALIAC dataset (Only ADLs, hip)

h) FARSEEING dataset (only falls)

Fig. 4. Averaged Power spectrum of the acceleration magnitude for ADLs and falls for different datasets containing data captured on the waist.

above 5 Hz. These conclusions are coherent with those preceding works that analyzed in the frequency domain the dynamics of conventional human movements. Thus, the recommendation of using a sampling rate of 20 Hz (and not higher than 40 or 50 Hz) for Human Activity Recognition systems can be extended to fall detection applications.

Funding

This research was funded by the Andalusian Regional Government (-Junta de Andalucía-) under grants FEDER UMA18-FEDERJA-022 and PAIDI P18-RT-1652, and by the Universidad de Málaga, Campus de Excelencia Internacional Andalucia Tech.

CRediT authorship contribution statement

José Antonio Santoyo-Ramón: Conceptualization, Software, Formal analysis, Investigation, Methodology, Writing – review & editing. **Eduardo Casilari:** Conceptualization, Data curation, Formal analysis, Funding acquisition, Investigation, Methodology, Project administration, Resources, Supervision, Writing – original draft. **José Manuel Cano-García:** Supervision, Validation, Visualization, Writing – review & editing.

Declaration of Competing Interest

The authors declare that they have no known competing financial interests or personal relationships that could have appeared to influence the work reported in this paper.

Acknowledgement

Funding for open access charge: Universidad de Malaga / CBUA.

References

[1] J. Sri-on, G.P. Tirrell, J.F. Bean, L.A. Lipsitz, S.W. Liu, Revisit, Subsequent Hospitalization, Recurrent Fall, and Death Within 6 Months After a Fall Among Elderly Emergency Department Patients, Ann. Emerg. Med. 70 (4) (2017) 516–521. e2, https://doi.org/10.1016/j.annemergmed.2017.05.023.

[2] T. Nguyen Gia, V.K. Sarker, I. Tcarenko, A.M. Rahmani, T. Westerlund, P. Liljeberg, H. Tenhunen, Energy efficient wearable sensor node for IoT-based fall detection systems, Microprocess. Microsyst. 56 (2018) 34–46, https://doi.org/10.1016/j.micpro.2017.10.014.

[3] D. Ajerla, S. Mahfuz, F. Zulkernine, A real-time patient monitoring framework for fall detection, Wirel. Commun. Mob. Comput. 2019 (2019) 1–13, https://doi.org/10.1155/2019/9507938.

[4] L. Gao, A.K. Bourke, J. Nelson, Evaluation of accelerometer based multi-sensor versus single-sensor activity recognition systems, Med. Eng. Phys. 36 (6) (2014) 779–785, https://doi.org/10.1016/j.medengphy.2014.02.012.

[5] M.H.M. Noor, Z. Salcic, Z.; K.I.K. Wang, Dynamic sliding window method for physical activity recognition using a single tri-axial accelerometer. In Proceedings of the 10th IEEE Conference on Industrial Electronics and Applications (ICIEA 2015); Institute of Electrical and Electronics Engineers Inc.: Auckland, New Zealand, June 15-17, 2015; pp. 102–107, doi: 10.1109/ICIEA.2015.7334092.

[6] P. Bet, P.C. Castro, M.A. Ponti, Fall detection and fall risk assessment in older person using wearable sensors: A systematic review, Int. J. Med. Inform. 130 (2019), 103946, https://doi.org/10.1016/j.ijmedinf.2019.08.006.

[7] G. Sannino, I. De Falco, G. De Pietro, A supervised approach to automatically extract a set of rules to support fall detection in an mHealth system, Appl. Soft Comput. J. 34 (2015) 205–216, https://doi.org/10.1016/j.asoc.2015.04.060.

[8] S. Fudickar, A. Lindemann, B. Schnor, B. Threshold-based Fall Detection on Smart Phones. In Proceedings of the Proceedings of the 7th International Conference on Health Informatics (HEALTHINF'2014); Angers, France, March 3-6, 2014, doi: 10.5220/0004795803030309.

[9] K.C. Liu, C.Y. Hsieh, S.P. Hsu, C.T. Chan, Impact of Sampling Rate on Wearable-Based Fall Detection Systems Based on Machine Learning Models, IEEE Sens. J. 18 (23) (2018) 9882–9890, https://doi.org/10.1109/JSEN.2018.2872835.

[10] N. Zurbuchen, A. Wilde, P. Bruegger, A Machine Learning Multi-Class Approach for Fall Detection Systems Based on Wearable Sensors with a Study on Sampling Rates Selection, Sensors 21 (2021) 938, https://doi.org/10.3390/S21030938.

[11] F. Ordóñez, D. Roggen, F.J. Ordóñez, D. Roggen, Deep Convolutional and LSTM Recurrent Neural Networks for Multimodal Wearable Activity Recognition, Sensors 16 (2016) 115, https://doi.org/10.3390/s16010115.

[12] M.M. Islam, O. Tayan, M.R. Islam, M.S. Islam, S. Nooruddin, M. Nomani Kabir, M. R. Islam, Deep Learning Based Systems Developed for Fall Detection: A Review, IEEE Access 8 (2020) 166117–166137, https://doi.org/10.1109/ACCESS.2020.3021943.

[13] J. Silva, D. Gomes, I. Sousa, J.S. Cardoso, Automated Development of Custom Fall Detectors: Position, Model and Rate Impact in Performance, IEEE Sens. J. 20 (10) (2020) 5465–5472, https://doi.org/10.1109/JSEN.2020.2970994.

[14] G. Vavoulas, C. Chatzaki, T. Malliotakis, M. Pediaditis, The Mobiact dataset: Recognition of Activities of Daily living using Smartphones. In Proceedings of the International Conference on Information and Communication Technologies for Ageing Well and e-Health (ICT4AWE); Rome, Italy, April 21-22, 2016, doi: 10.5220/0005792401430151.

[15] A. Sucerquia, J.D. López, J.F. Vargas-bonilla, SisFall: A Fall and Movement Dataset, Sensors 198 (2017) 1–14, https://doi.org/10.3390/s17010198.

[16] E. Casilari, J.A. Santoyo-Ramón, J.M. Cano-García, I.M. Pires, On the Heterogeneity of Existing Repositories of Movements Intended for the Evaluation of Fall Detection Systems, J. Healthc. Eng. 2020 (2020) 1–36, https://doi.org/10.1155/2020/6622285.

[17] E. Casilari, J.A. Santoyo-Ramón, J.M. Cano-García, Analysis of public datasets for wearable fall detection systems, Sensors 17 (7) (2017) 1513, https://doi.org/10.3390/s17071513.

[18] Kaluža, B.; Mirchevska, V.; Dovgan, E.; Luštrek, M. An Agent-based Approach to Care in Independent Living. In Proceedings of the 1st International Joint Conference on Ambient Intelligence 2010 (AmI-10); Malaga, Spain, November 10-12, 2010; pp. 177–186.

[19] F.T. Wang, H.-L. Chan, M.H. Hsu, C.K. Lin, P.K. Chao, Y.J. Chang, Threshold-based fall detection using a hybrid of tri-axial accelerometer and gyroscope, Physiol. Meas. 39 (10) (2018) 105002, https://doi.org/10.1088/1361-6579/aae0eb.

[20] S. Kozina, H. Gjoreski, M. Gams, M. Luštrek, Three-layer activity recognition combining domain knowledge and meta-classification, J. Med. Biol. Eng. 33 (2013) 406–414, https://doi.org/10.5405/jmbe.1321.

[21] B. Kwolek, M. Kepski, Human fall detection on embedded platform using depth maps and wireless accelerometer, Comput. Methods Programs Biomed. 117 (3) (2014) 489–501, https://doi.org/10.1016/j.cmpb.2014.09.005.

[22] T. Vilarinho, B. Farshchian, D.G. Bajer, O.H. Dahl, I. Egge, I.; S.S. Hegdal, A. Lones, J.N. Slettevold, S.M. Weggersen, A Combined Smartphone and Smartwatch Fall Detection System. In Proceedings of the 2015 IEEE International Conference on Computer and Information Technology; Ubiquitous Computing and Communications; Dependable, Autonomic and Secure Computing; Pervasive Intelligence and Computing (CIT/IUCC/DASC/PICOM); Liverpool, UK, October 26-28, 2015; pp. 1443–1448, doi:10.1109/CIT/IUCC/DASC/PICOM.2015.216.

[23] T.R. Mauldin, M.E. Canby, V. Metsis, A.H.H. Ngu, C.C. Rivera, SmartFall: A Smartwatch-Based Fall Detection System Using Deep Learning, Sensors 18 (2018) 3363, https://doi.org/10.3390/s18103363.

[24] M. Ahmed, N. Mehmood, A. Nadeem, A. Mehmood, K. Rizwan, Fall detection system for the elderly based on the classification of shimmer sensor prototype data, Healthc. Inform. Res. 23 (2017) 147–158, https://doi.org/10.4258/hir.2017.23.3.147.

[25] J. Klenk, L. Schwickert, L. Palmerini, S. Mellone, A. Bourke, E.A.F. Ihlen, N. Kerse, K. Hauer, M. Pijnappels, M. Synofzik, K. Srulijes, W. Maetzler, J.L. Helbostad, W. Zijlstra, K. Aminian, C. Todd, L. Chiari, C. Becker, The FARSEEING real-world fall repository: a large-scale collaborative database to collect and share sensor signals from real-world falls, Eur. Rev. Aging Phys. Act. 13 (1) (2016), https://doi.org/10.1186/s11556-016-0168-9.

[26] D. Micucci, M. Mobilio, P. Napoletano, UniMiB SHAR: a new dataset for human activity recognition using acceleration data from smartphones, Appl. Sci. 7 (2017), https://doi.org/10.3390/app7101101.

[27] K. Frank, M.J. Vera Nadales, P. Robertson, T. Pfeifer, Bayesian recognition of motion related activities with inertial sensors. In Proceedings of the 12th ACM International Conference on Ubiquitous Computing; ACM: Copenhagen, Denmark, September 26–29, 2010; pp. 445–446, doi:10.1145/1864431.1864480.

[28] A. Wertner, P. Czech, V. Pammer-Schindler, An Open Labelled Dataset for Mobile Phone Sensing Based Fall Detection. In Proceedings of the 12th EAI International Conference on Mobile and Ubiquitous Systems: Computing, Networking and Services (MOBIQUITOUS 2015); Coimbra, Portugal, July 22-24, 2015; pp. 277–278, doi:10.4108/eai.22-7-2015.2260160.

[29] F. Luna-Perejón, L. Muñoz-Saavedra, J. Civit-Masot, A. Civit, M. Domínguez-Morales, AnkFall—Falls, Falling Risks and Daily-Life Activities Dataset with an Ankle-Placed Accelerometer and Training Using Recurrent Neural Networks, Sensors 2021 (1889) 21, https://doi.org/10.3390/s21051889.

[30] O. Ojetola, E. Gaura, J. Brusey, Data Set for Fall Events and Daily Activities from Inertial Sensors. In Proceedings of the 6th ACM Multimedia Systems Conference (MMSys'15); Portland, Oregon, USA, March 18-20, 2015; pp. 243–248, doi: 10.1145/2713168.2713198.

[31] T.H. Tran, T.L. Le, D.T. Pham, V.N. Hoang, V.M. Khong, Q.T. Tran, T.S. Nguyen, C. Pham, A multi-modal multi-view dataset for human fall analysis and preliminary investigation on modality. In Proceedings of the 24th International Conference on Pattern Recognition (ICPR'18); Institute of Electrical and Electronics Engineers Inc.: Beijing, China, August 24-28, 2018; pp. 1947–1952, doi:10.1109/ICPR.2018.8546308.

[32] V. Cotechini, A. Belli, L. Palma, M. Morettini, L. Burattini, P. Pierleoni, A dataset for the development and optimization of fall detection algorithms based on wearable sensors, Data Br 103839 (2019), https://doi.org/10.1016/j.dib.2019.103839.

[33] S.S. Saha, S. Rahman, M.J. Rasna, A.K.M. Mahfuzul Islam, M.A Rahman Ahad, DU-MD: An Open-Source Human Action Dataset for Ubiquitous Wearable Sensors. In Proceedings of the 2018 Joint 7th International Conference on Informatics, Electronics & Vision (ICIEV) and 2018 2nd International Conference on Imaging,

Vision & Pattern Recognition (icIVPR); IEEE: Fukuoka, Japan, June 25-29, 2018; pp. 567–572, doi:10.1109/ICIEV.2018.8641051.

[34] A.T. Özdemir, B. Barshan, Detecting Falls with Wearable Sensors Using Machine Learning Techniques, Sensors 14 (2014) 10691–10708, https://doi.org/10.3390/s140610691.

[35] M. Saleh, M. Abbas, R.B. Le Jeannes, FallAllD: An Open Dataset of Human Falls and Activities of Daily Living for Classical and Deep Learning Applications, IEEE Sens. J. 21 (2) (2021) 1849–1858, https://doi.org/10.1109/JSEN.2020.3018335.

[36] O. Aziz, M. Musngi, E.J. Park, G. Mori, S.N. Robinovitch, A comparison of accuracy of fall detection algorithms (threshold-based vs. machine learning) using waist-mounted tri-axial accelerometer signals from a comprehensive set of falls and non-fall trials, Med. Biol. Eng. Comput. 55 (1) (2017) 45–55, https://doi.org/10.1007/s11517-016-1504-y.

[37] X. Yu, J. Jang, S. Xiong, A Large-scale Open Motion Dataset (KFall) and Benchmark Algorithms for Detecting Pre-impact Fall of the Elderly Using Wearable Inertial Sensors, Front. Aging Neurosci. 13 (2021), 692865, https://doi.org/10.3389/FNAGI.2021.692865.

[38] C. Medrano, R. Igual, I. Plaza, M. Castro, C. Lovis, Detecting falls as novelties in acceleration patterns acquired with smartphones, PLoS One 9 (4) (2014) e94811, https://doi.org/10.1371/journal.pone.0094811.

[39] S. Gasparrini, E. Cippitelli, S. Spinsante, E. Gambi, A depth-based fall detection system using a Kinect® sensor, Sensors 14 (2014) 2756–2775, https://doi.org/10.3390/s140202756.

[40] E. Casilari, J.A. Santoyo-Ramón, J.M. Cano-García, S. Federici, Analysis of a Smartphone-Based Architecture with Multiple Mobility Sensors for Fall Detection, PLoS One 11 (12) (2016) e0168069, https://doi.org/10.1371/journal.pone.0168069.

[41] L. Martínez-Villaseñor, H. Ponce, J. Brieva, E. Moya-Albor, J. Núñez-Martínez, C. Peñafort-Asturiano, UP-Fall Detection Dataset: A Multimodal Approach, Sensors 2019 (1988) 19, https://doi.org/10.3390/s19091988.

[42] E. Casilari, M. Álvarez-Marco, F. García-Lagos, A Study of the use of gyroscope measurements in wearable fall detection systems, Symmetry (Basel) 12 (2020) 649, https://doi.org/10.3390/SYM12040649.

[43] C.Y. Hsieh, K.C. Liu, C.N. Huang, W.C. Chu, C.T. Chan, Novel Hierarchical Fall Detection Algorithm Using a Multiphase Fall Model, Sensors 17 (2017) 307, https://doi.org/10.3390/s17020307.

[44] X. Yu, Approaches and principles of fall detection for elderly and patient. In Proceedings of the 10th International Conference on e-health Networking, Applications and Services (HealthCom 2008); Singapore, July 7-9, 2008; pp. 42–47, doi:10.1109/HEALTH.2008.4600107.

[45] Mathworks. Deep Learning Toolbox Documentation Available online: https://es.mathworks.com/help/deeplearning/index.html (accessed on Oct 21, 2021).

[46] Y.S. Delahoz, M.A. Labrador, Survey on fall detection and fall prevention using wearable and external sensors, Sensors 14 (2014) 19806–19842, https://doi.org/10.3390/s141019806.

[47] X. Wang, J. Ellul, G. Azzopardi, Elderly Fall Detection Systems: A Literature Survey, Front. Robot. AI 7 (2020), https://doi.org/10.3389/frobt.2020.00071.

[48] B. Andò, S. Baglio, S. Castorina, R. Crispino, V. Marletta, Advanced Solutions Aimed at the Monitoring of Falls and Human Activities for the Elderly Population, Technologies 7 (2019) 59, https://doi.org/10.3390/technologies7030059.

[49] L. Ren, Y. Peng, Research of fall detection and fall prevention technologies: A systematic review, IEEE Access 7 (2019) 77702–77722, https://doi.org/10.1109/ACCESS.2019.2922708.

[50] R. Broadley, J. Klenk, S. Thies, L. Kenney, M. Granat, R.W. Broadley, J. Klenk, S. B. Thies, L.P.J. Kenney, M.H. Granat, Methods for the Real-World Evaluation of Fall Detection Technology: A Scoping Review, Sensors 18 (2018) 2060, https://doi.org/10.3390/s18072060.

[51] H. Gjoreski, M. Luštrek, M. Gams, Accelerometer placement for posture recognition and fall detection. In Proceedings of the 7th International Conference on Intelligent Environments (IE 2011); Nottingham, UK, July 25-28, 2011; pp. 47–54, doi:10.1109/IE.2011.11.

[52] 52. J. Dai, X. Bai, Z. Yang, Z. Shen, D. Xuan, PerFallD: A pervasive fall detection system using mobile phones. In Proceedings of the 8th IEEE International Conference on Pervasive Computing and Communications Workshops (PERCOM Workshops); Mannheim, Germany, March 29 - April 2, 2010; pp. 292–297, doi:10.1109/PERCOMW.2010.5470652.

[53] M. Kangas, A. Konttila, P. Lindgren, I. Winblad, T. Jämsä, Comparison of low-complexity fall detection algorithms for body attached accelerometers, Gait Posture 28 (2008) 285–291, https://doi.org/10.1016/j.gaitpost.2008.01.003.

[54] S.H. Fang, Y.C. Liang, K.M. Chiu, Developing a mobile phone-based fall detection system on android platform, in: In Proceedings of the Computing, Communications and Applications Conference (ComComAp); Hong Kong, China, IEEE, 2012, pp. 143–146.

[55] H. Leutheuser, D. Schuldhaus, B.M. Eskofier, I.P. Androulakis, Hierarchical, Multi-Sensor Based Classification of Daily Life Activities: Comparison with State-of-the-Art Algorithms Using a Benchmark Dataset, PLoS One 8 (10) (2013) e75196, https://doi.org/10.1371/journal.pone.0075196.

[56] M.J. Mathie, A.C.F. Coster, N.H. Lovell, B.G. Celler, Accelerometry: Providing an integrated, practical method for long-term, ambulatory monitoring of human movement, Physiol. Meas. 25 (2) (2004) R1–R20, https://doi.org/10.1088/0967-3334/25/2/r01.

[57] E.K. Antonsson, R.W. Mann, The frequency content of gait, J. Biomech. 18 (1) (1985) 39–47, https://doi.org/10.1016/0021-9290(85)90043-0.

[58] D.A. Winter, Biomechanics and Motor Control of Human Movement: Fourth Edition, Biomech. Mot. Control Hum. Mov. Fourth Ed. 7 (2009) 1–370, https://doi.org/10.1002/9780470549148.

[59] H.P. Nguyen, F. Ayachi, C. Lavigne-Pelletier, M. Blamoutier, F. Rahimi, P. Boissy, M. Jog, C. Duval, Auto detection and segmentation of physical activities during a Timed-Up-and-Go (TUG) task in healthy older adults using multiple inertial sensors, J. Neuroeng. Rehabil. 12 (2015) 36, https://doi.org/10.1186/s12984-015-0026-4.

[60] C.V.C. Bouten, K.T.M. Koekkoek, M. Verduin, R. Kodde, J.D. Janssen, A triaxial accelerometer and portable data processing unit for the assessment of daily physical activity, IEEE Trans. Biomed. Eng. 44 (1997) 136–147, https://doi.org/10.1109/10.554760.